CHEMISTRY
A European Journal

A Journal of
ChemPubSoc Europe

Accepted Article

Title: Hydrazide-hydrazone Small Molecules as AIEgens: Illuminating Mitochondria in Cancer Cells

Authors: Sohan Patil, Shalini Pandey, Amit Singh, Mithun Radhakrishna, and Sudipta Basu

To be cited as: *Chem. Eur. J.* 10.1002/chem.201901074

Link to VoR: http://dx.doi.org/10.1002/chem.201901074

Supported by
ACES

WILEY-VCH

10.1002/chem.201901074

COMMUNICATION

WILEY-VCH

Hydrazide-hydrazone Small Molecules as AIEgens: Illuminating Mitochondria in Cancer Cells

Sohan Patil,[a] Shalini Pandey,[a] Amit Singh,[b] Mithun Radhakrishna,[c] and Sudipta Basu*[b]

Abstract: Aggregation induced emission probes (AIEgens) have gained lots of attention as interesting tools for ample biomedical applications especially bio-imaging due to their brightness and photo-stability. Numerous AIEgens have been developed for lighting up the sub-cellular organelles to understand their forms and functions in healthy as well as diseased states like cancer. However, there is a serious absence of easily synthesizable, biocompatible small molecules for illuminating mitochondria (powerhouses) inside cells. To address this, in this report we describe an easy and short synthesis of novel biocompatible hydrazide-hydrazone based small molecules with remarkable aggregation-induced emission (AIE) property. These small molecule AIEgens showed hitherto unobserved AIE property due to dual intra-molecular H-bonding confirmed by theoretical calculation, pH and temperature dependent fluorescence and X-ray crystallography studies. Confocal microscopy showed that these AIEgens were internalized into the HeLa cervical cancer cells without showing any cytotoxicity. One of the AIEgens was tagged with triphenylphosphine (TPP) moiety which successfully localized into mitochondria of HeLa cells selectively compared to L929 non-cancerous fibroblast cells. These unique hydrazide-hydrazone based biocompatible AIEgens can serve as powerful tools to illuminate multiple sub-cellular organelles to elucidate their forms and functions in cancer cells for next-generation biomedical applications.

In last decade, aggregation-induced emission luminogens (AIEgens) have emerged as powerful tools to develop chemical sensors, optoelectronic devices and theranostic probes for biomedical applications due to their brightness and excellent photo-stability.[1-6] However, till date, tetraphenylethylene (TPE) and hexaphenylsilole (HPS) moieties are extensively explored as effective AIEgens despite their tedious synthetic steps and highly hydrophobic nature leading to incompatibility for biological applications.[7-10] To introduce biocompatibility for imaging and therapy, majority of the AIEgens was tagged with hydrophilic moieties to decorate hydrophobic AIE core through multiple synthetic steps.[11-15] Recently, numerous biocompatible AIEgens have been developed for *in vitro* cellular imaging, especially to visualize intra-cellular organelles.[16-21] Mitochondrion is one of

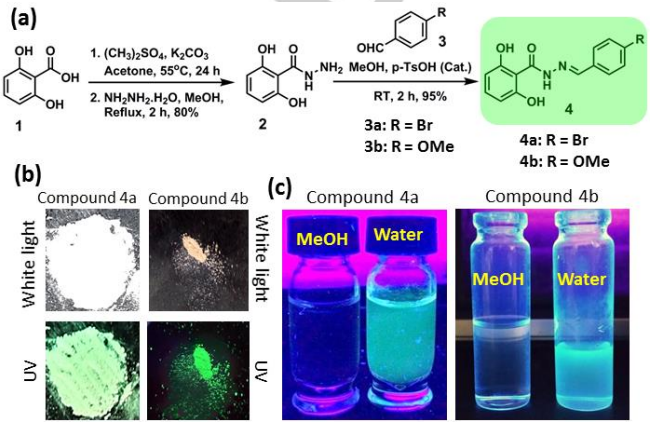

Figure 1. (a) Synthetic scheme of hydrazide-hydrazone molecules. (b) Fluorescence emission images of compound 4a and 4b under UV lights and white light in solid state. (c) Images of AIE property of compound 4a and 4b in water and in methanol.

the most important organelles which orchestrate several cellular functions, hence implicated in different diseased states including cancer.[22-24] As a result, visualizing mitochondria inside the cancer cells is of utmost importance to understand their form and function in cancer progression and management. Despite several TPE and HPS-based AIEgens have been explored lately,[25-30] there is still a serious lack of biocompatible small molecule based AIEgens for visualization of mitochondria in cancer cells.

To address this, in this manuscript, for the first time, we have developed hydrazide-hydrazone based small molecules through simple and concise synthetic steps, which showed remarkable aggregation-induced emission (AIE) properties in water as well as in solid state by dual intra-molecular H-bonding. This dual H-bonding mediated restriction in intra-molecular motions (RIM) for AIE properties was confirmed by temperature and pH-dependent fluorescence quenching studies, ^{1}H NMR spectroscopy and theoretical calculations as well as X-ray crystallography. One of the hydrazide-hydrazone based AIEgens was decorated with positively charged triphenylphosphine (TPP) to illuminate mitochondria in HeLa cervical cancer cells compared to L929 non-cancerous fibroblast cells. These hydrazide-hydrazone small molecule AIEgens showed remarkable biocompatibility by demonstrating negligible cell killing even at significantly high concentrations. This novel biocompatible AIEgens can act as platform probes to further illuminate several intra-cellular organelles and bio-targets.

The synthetic scheme of hydrazide-hydrazone derivatives (**4**) is shown in Figure 1a. 2,6-dihydroxybenzoic acid was reacted with dimethyl sulfate in presence of potassium carbonate as base at 55 °C in acetone for 24 h to obtain 2,6-dihydroxy benzoic acid methyl ester which was subsequently reacted with hydrazine monohydrate in methanol at refluxing condition to afford 2,6-dihydroxy benzohydrazide (**2**) in 80% overall yield. Finally,

[a] S. Patil, S. Pandey
Department of Chemistry
Indian Institute of Science Education and Research (IISER)-Pune,
Dr. Homi Bhabha Road, Pashan, Pune, Maharashtra, 411008, India.
[b] A. Singh, Prof. S. Basu
Discipline of Chemistry
Indian Institute of Technology (IIT)-Gandhinagar, Palaj,
Gandhinagar, Gujarat, 382355, India.
Email: Sudipta.basu@iitgn.ac.in
[c] Prof. M. Radhakrishna
Discipline of Chemical Engineering, Indian Institute of Technology
(IIT)-Gandhinagar, Palaj, Gandhinagar, Gujarat, 382355, India.

Supporting information for this article is given via a link at the end of the document.

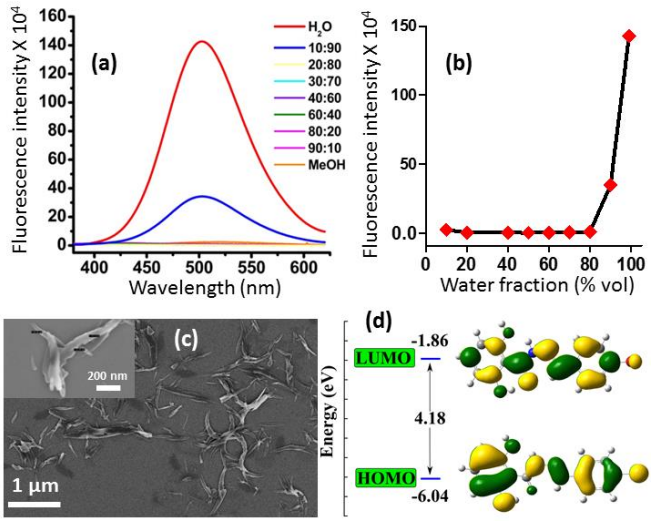

Figure 2. (a) Fluorescence emission spectra of compound 4a in different methanol: water ratios. (b) Fluorescence emission intensity (λ_{max} = 502 nm) versus water fraction graph of compound 4a in different methanol: water mixture. (c) FESEM images of compound 4a in water. (d) Schematic diagram of the energy level difference between the HOMOs and LUMOs of compound 4a, estimated from DFT computation and the isodensity surface plots of the frontier molecular orbitals (FMOs) with isovalue of 0.02 au.

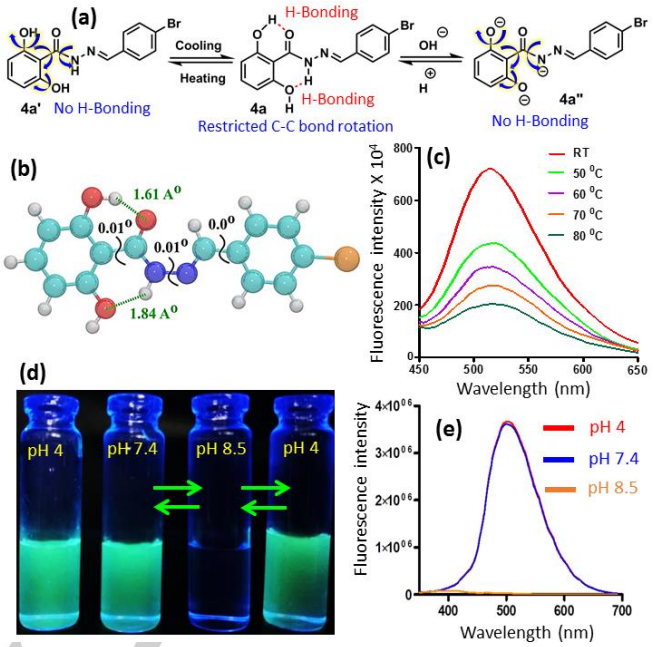

Figure 3. (a) Scheme of H-bonding disruption of compound 4a in temperature and pH change. (b) Optimized geometry of compound 4a obtained from B3LYP/6-31G* computation. Black zig-zag lines showing values for the respective dihedral angles (in degree) whereas hydrogen bonding is shown in green dotted lines. Atoms of C, O, N, Br and H are shown in cyan, red, blue, orange and white colors, respectively. (c) Temperature dependent change in fluorescence emission spectra of compound 4a in water. (d, e) Images and fluorescence emission spectra of compound 4a in different pH.

different 4-substituted benzaldehydes (**3a, b**) were reacted with compound **2** in presence of catalytic *p*-toluenesulfonic acid (*p*-TsOH) to afford hydrazide-hydrazone derivatives (**4a, b**) in 95% yield. All the intermediates and final compounds were characterized by NMR (^{1}H and ^{13}C) and mass spectroscopy (HR- MS) (Figure S1-S9).[31] Interestingly, all the hydrazidhydrazone derivatives (**4a, b**) showed remarkable fluorescence emission under long range of UV light in solid state (Figure 1b). However, no fluorescence emission was observed under white visible light. Similarly, compounds **4a, b** showed no fluorescence emission in methanol. On the other hand, both the hydrazide-hydrazone derivatives (**4a, b**) showed remarkable fluorescence emission in water (Figure 1c). This observation clearly indicated the aggregation-induced emission (AIE) properties of compound **4**.

To evaluate the exact solvent ratio of aggregation induction, we dissolved compound **4a** in methanol and gradually titrated with increased amount of water. There was no fluorescence signal observed till methanol: water = 20:80 (v/v). However, compound **4a** showed an increase in fluorescence emission intensity at methanol: water = 10:90 (v/v) at λ_{max} = 502 nm, which increased significantly at 100 % water (Figure 2a,b, Figure S10a). The UV-Vis spectra of compound **4a** showed absorption maxima at λ_{max} = 322 nm in methanol and water (Figure S10b), indicative of a large Stokes shift of 180 nm with negligible overlap between absorption and emission spectra, which is highly suited for fluorescence imaging. Similarly, compound **4b** showed remarkable fluorescence emission intensity increment (λ_{max} = 492 nm) in water compared to methanol due to aggregation (Figure S11). The aggregation of compound **4a** in water was further validated by dynamic light scattering (DLS), which demonstrated that the mean hydrodynamic diameter of aggregated structure in water to be 706 nm (Figure S12). In contrast, compound **4a** showed very small hydrodynamic diameter (~ 3.5 nm) in methanol indicating negligible aggregation (Figure S12). We also visualized the aggregation of compound **4a** by scanning electron microscopy. The FESEM images evidently showed that compound **4a** aggregated into 2D-sheet like structures in water, whereas no such significant aggregation was found in methanol (Figure 2c). To confirm the remarkable enhancement in the fluorescence emission intensity of compound **4a** and **4b** due to the effect of aggregation, we assessed the fluorescence emission in a concentration dependent manner. As expected, the fluorescence emission intensity of compound **4a** and **4b** were increased continuously after increasing the concentration of the compounds in water (Figure S13). We also performed fluorescence life time experiment which revealed that compound **4a** and **4b** had 1.97 and 1.50 ns of fluorescence life time respectively which is little less compared to Rhodamine 123, a traditionally used commercial mitochondria imaging agent (Figure S14).[32] The fluorescence quantum yield of compound **4a** and **4b** were found to be 12.2% and 5.4 % respectively which are comparable with the structurally similar imine compounds as well as much higher to Rhodamine 123 (~ 0.9%).[32,33] Subsequently the Frontier molecular orbitals and the energy gap between HOMOs and

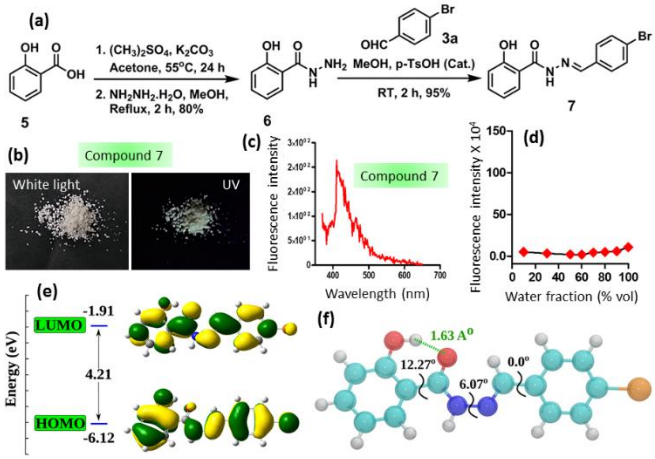

Figure 4. (a) Scheme for the synthesis of compound 7. (b) Solid state fluorescence images of compound 7 under white light and UV. (c) Fluorescence spectra of compound 7 in water. (d) Fluorescence emission intensity versus water fraction graph of compound 7 in different methanol: water mixture.(e) Schematic diagram of the energy level difference between the HOMOs and LUMOs of compound 7, estimated from DFT computation and the isodensity surface plots of the frontier molecular orbitals (FMOs) with isovalue of 0.02 au. (f) Optimized geometry of compound 7 obtained from B3LYP/6-31G* computation. Black zig-zag lines showing values for the respective dihedral angles (in degree) whereas hydrogen bonding is shown in green dotted lines. The atoms of C, O, N, Br and H are shown in cyan, red, blue, orange and white colors, respectively.

LUMOs of compound **4a** was calculated by Density functional theory (DFT), which revealed the energy gap was ~ 4.18 eV (~ 300 nm) correlating with the wavelength of UV-Vis absorbance (Figure 2d).

We hypothesize dual intra-molecular H-bonding as the guiding factor for this hitherto unobserved AIE property for these novel hydrazide-hydrazone small molecules leading to restriction in intra-molecular motion (RIM) (Figure 3a). To confirm our hypothesis, we performed theoretical calculation using Gaussian 09 program on compound **4a**.[34] 3D coordinates of compound **4a** were generated from the crystal structure of 4-N, N-dimethylaminoaniline salicylaldehyde reported by Feng et. al.[27] with a few modifications. The geometries were then additionally optimized by the B3LYP[35] hybrid density functional with 6-31G* Gaussian basis set. The presence of water was mimicked with polarizable continuum model using the integral equation formalism variant.[36] The geometry of the optimized molecular structure of compound **4a** showed that all the atoms were in the same plane (Figure 3b) and confirmed the proposed dual intra-molecular H-bonding.

Inter- or intra-molecular H-bonding are weak supramolecular forces which can be disrupted by increasing the temperature of the medium.[37] Moreover, ^{1}H NMR spectroscopy has emerged as one of the tools to probe the presence of inter- and intra-molecular H-bonding.[38] Hence, we performed temperature dependent ^{1}H NMR spectroscopy of compound **4a** from 25°C to 80°C and monitored the H-bonded proton peaks at 12.07 (-OH) and 11.81 ppm (-NH). Remarkably, we observed the gradual broadening of both these peaks while increasing the temperature from 25°C to 80°C (Figure S15). This observation is in complete agreement with our previous study.[39] To validate our hypothesis further, we performed temperature dependent fluorescence spectroscopy on compound **4a** in water. It was observed that, with gradual increase in temperature from 25°C to 80°C, the intensity of fluorescence emission was gradually decreased by 3.5 folds (Figure 3c) due to the destruction of H-bonding in structure **4a'**. Interestingly, this fluorescence quenching phenomena was found to be reversible.

Inter- and intra-molecular H-bonding leading to AIE property is highly sensitive to the pH of the medium.[40] Hence, we perturbed intra-molecular H-bonding by increasing the pH of the medium from 7.4 to 8.5. Interestingly, it was observed that compound **4a** lost its fluorescence property completely (Figure 3d) leading to the destruction of H-bonding in structure **4a"**. On the other hand, decreasing the pH from 8.5 to 7.4 resumed the fluorescence property into compound **4a** which even retained at much lower pH = 4 (Figure 3d,e). As expected, compound **4b** also showed similar pH dependent fluorescence property (Figure S16). For future mitochondrial imaging, the AIE probe should be fluorescent at pH 7.8-8.0 which mimics the mitochondria matrix. Hence, we assessed the AIE property of compound **4a** at pH = 7.8 and 8.0. It was observed that the fluorescence intensity of compound **4a** was marginally reduced at pH = 7.8 and 8.0 compared to pH = 7.4 (Figure S17). Also 9.3% quantum yield was calculated for compound **4a** at pH = 7.8 which indicated that compound **4a** is suitable for mitochondrial bio-imaging. We further evaluated the effect of solvents on the AIE property of compound **4a** and **4b**. To our surprise, compound **4a** showed high and marginal AIE property in water and toluene respectively (Figure S18a,b). However, compound **4a** showed no AIE property in other solvents like hexane, THF and DMSO. Similarly, compound **4b** also demonstrated AIE property in water only (Figure S18c,d). This theoretical calculation along with temperature and pH dependent reversible fluorescence quenching-regaining clearly confirmed the role of intra-molecular H-bonding in inducing AIE property in compound **4a**. However, we anticipate that the amphiphilicity of compound **4a** and **4b** also played a crucial role in inducing AIE property, which needs to be explored carefully in future to understand the exact mechanism.

One of the plausible mechanisms of this photophysical property of compound **4a, b** could be exited state intramolecular proton transfer (ESIPT).[41,42] To validate the involvement of ESIPT as well as the role of dual intra-molecular H-bonding in triggering AIE property in compound **4a**, we have synthesized mono-hydroxy hydrazide-hydrazone compound **7** starting from 2-hydroxybenzoic acid (**5**) by the same synthetic strategy via 2-hydroxy benzohydrazide (**6**) (Figure 4a). All the compounds were chemically characterized by NMR (^{1}H and ^{13}C) and HR-MS spectroscopy (Figure S19-S24). Interestingly, compound **7** showed negligible fluorescence property in solid state as well as in water (Figure 4b,c). We further evaluated the change in fluorescence property in methanol/water mixture. Negligible increase in fluorescence intensity of compound **7** was observed in 100% methanol to 100% water (Figure 4d and Figure S25). The Frontier molecular orbitals and the energy gap between HOMOs and LUMOs of compound **7** were calculated by DFT

10.1002/chem.201901074

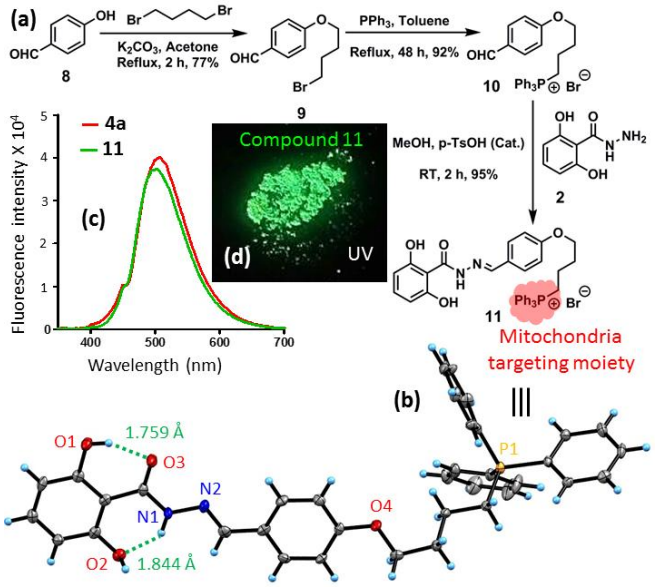

Figure 5. (a) Synthetic scheme of mitochondria targeted hydrazide-hydrazone molecule (11). (b) ORTEP diagram of compound 11 with 50% thermal ellipsoids. Solvent and counter ions are removed for clarity. (c) Fluorescence emission spectra of compound 11 in water. (d) Fluorescence emission image of compound 11 in solid state under UV light.

which showed the energy gap was ~ 4.21 eV (~ 295 nm)(Figure 4e) comparable to the energy gap in compound **4a**. Finally, we executed theoretical calculations using Gaussian 09 program on compound **7**. Most interestingly, the optimized molecular geometry of compound **7** showed the dihedral angle of the mono-intramolecular H-bonded moiety was increased to ~12.3º (Figure 4f) compared to nearly 0º dihedral angle found in compound **4a**. This clearly indicated that single intra-molecular H-bonding is not sufficient to maintain coplanarity along the largest molecular axis in compound **7** leading to lack of aggregated structure with negligible AIE property. Moreover, in our previous study, we synthesized O-phenyl-hydrazide-hydrazone analogue of compound **7**, which showed no AIE property in solid state as well as in solution.[43] These solid state fluorescence, water titration studies and theoretical structure optimization clearly confirmed that (a) ESIPT is not the mechanism involved and (b) dual intra-molecular H-bonding is critical to maintain the planarity in compound **4a, b** to induce aggregation to show AIE property. However, at this point, the exact mechanism of this photophysical phenomena in these novel hydrazide-hydrazone based small molecules is elusive and we are exploring this area currently.

To be successful in bio-imaging, the hydrazide-hydrazone AIE probes should be biocompatible. Hence, we evaluated the *in vitro* cytotoxicity of compound **4a** and **4b** in HeLa cervical cancer cells at 48 h post-incubation in a dose dependent manner. The cell viability was measured by MTT assay which showed compound **4a** induced only 94.2 ± 4.5 %, 97.4 ± 2.2 % and 91.8 ± 5.6 % cell viability at 12.5, 25 and 50 μM concentrations respectively (Figure S26a). Similarly, compound **4b** also demonstrated 99.5 ± 0.4 %, 95.3 ± 2.7 % and 94.1 ± 2.2 % cell viabilities at 12.5, 25 and 50 μM concentrations (Figure S26a). To evaluate the biocompatibility in non-cancerous cells, we incubated fibroblast L929 cells with compound **4a** and **4b** in a concentration dependent manner for 24 h. The MTT assay revealed that compound **4a** induced only 97.6 ± 1.4%, 94.3 ± 1.7% and 86.3 ± 1.8% cell viability at 12.5, 25 and 50 μM concentrations respectively (Figure S26b). Similarly, compound **4b** also showed only 94.6 ± 4.8%, 91.3 ±5.6% and 83.2 ± 2.3% cell viability at 12.5, 25 and 50 μM concentrations respectively. This cell viability assay confirmed that compound **4a** and **4b** were not at all toxic to the cancer cells as well as non-cancerous fibroblast cells, hence can be used for bio-imaging.

To evaluate the effectiveness of compound **4a** and **4b** in sub-cellular mitochondria imaging in cancer cells, we treated HeLa cells with both the compounds at 10 μM concentrations for 12 h. Mitochondria were co-stained by MitoTracker Red dye and the live cells were visualized by fluorescence confocal microscopy. Confocal images in Figure S26c evidently showed that both compounds **4a** and **4b** were internalized into the cells successfully and localized into mitochondria leading to the generation of yellow regions by overlapping green and red fluorescence signals. However, both the compounds were also localized into nucleus of the cells significantly. In fact, compound **4a** and **4b** showed non-specific sub-cellular localization which was non-effective in specific mitochondria labeling. Furthermore, to estimate the cancer cell specificity over non-cancerous cells, we incubated fibroblast L929 cells with compound **4a** and **4b** at 20 μM concentrations for 12 h. The nuclei of the cells were counter stained with blue fluorescence DAPI. The cells were then fixed and visualized by confocal microscopy. Surprisingly, the fluorescence microscopy images (Figure S27) hardly showed any sub-cellular green fluorescence signals, indicating that compound **4a** and **4b** barely internalized into L929 cells even after 12h. These confocal images confirmed that these novel AIE active hydrazide-hydrazone derivatives specifically internalized into HeLa cancer cells over L929 non-cancerous cells.

To overcome this challenge, we have synthesized hydrazide-hydrazone based molecule tagged with positively charged triphenylphosphonium (TPP) moiety for mitochondria targeting. 4-hydroxybenzaldehyde (**8**) was first reacted with excess 1,4-dibromobutane in presence of potassium carbonate as base in acetone in refluxing condition to obtain compound **9** in 77 % yield (Figure 5a). The bromine moiety was further replaced by triphenylphosphine in refluxing condition to obtain compound **10** in 92% yield. Finally, compound **10** was coupled with 2,6-dihydroxy benzohydrazide (**2**) in presence of *p*-TsOH as catalyst to obtain positively charged triphenylphosphonium tagged hydrazide-hydrazone (**11**) in 95% yield. NMR (^{1}H, ^{13}C and ^{31}P) and HR-MS were used to characterize all the compounds (Figure S28-S38). We also characterized the structure of compound **11** by X-ray crystallography (Figure 5b) which clearly confirmed the presence of proposed dual intra-molecular H-bonding correlating with the theoretical electronic structure in Figure 3b.We further assessed the photo-physical properties of compound **11** which showed fluorescence emission at λ_{max} = 500 nm in water as well as AIE in solid state under UV light (Figure 5c,d).

The viability of HeLa cells in presence of compound **11** after 48 h was determined by MTT assay in a dose dependent manner.

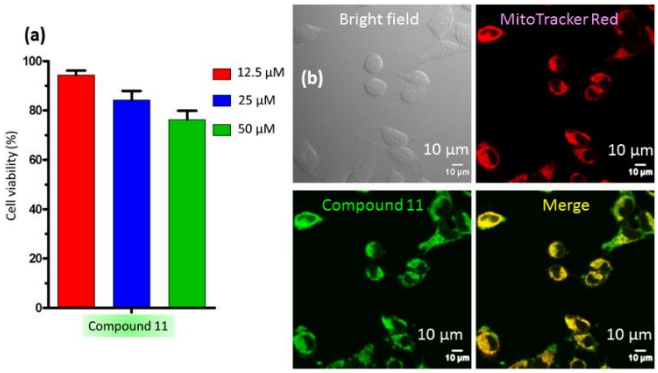

Figure 6. (a) Viability of HeLa cells after treatment with compound 11 in a dose dependent manner for 48 h by MTT assay. (b) CLSM images of HeLa cells after treatment with compound 11 for 12 h. Mitochondria were stained by MitoTracker Red. Scale bar = 10 µm.

This cell viability assay showed that compound **11** induced only 5.5± 1.8, 15.9±3.7 and 23.8±3.6 % cell death at 12.5, 25 and 50 µM concentrations respectively (Figure 6a). We also evaluated the biocompatibility of compound **11** in non-cancerous fibroblast L929 cells at 24 h post-incubation. The MTT assay revealed that compound **11** induced 92.0± 3.5%, 87.6 ± 1.4% and 76.1 ±1.9% cell viability at 12.5, 25 and 50 µM concentrations respectively (Figure S39a). These cell viability assays indicated that compound **11** is biocompatible for cervical cancer cells as well as non-cancerous fibroblast cells for imaging. Furthermore, compound **11** showed much better biocompatibility compared to the traditionally used Rhodamine 123 as mitochondria staining red fluorescent dye.[44,45]

To estimate its potential in mitochondria imaging, we treated HeLa cells with compound **11** at 10 µM concentration for 12 h, followed by staining mitochondria by MitoTracker Red. The confocal images of the live cells (Figure 6b) evidently showed that compound **11** homed into mitochondria of HeLa cells leading to yellow overlapping regions. Interestingly, hardly any green fluorescence signal was observed into nucleus of the HeLa cells, which confirmed the specific mitochondria imaging by compound **11**. We also visualized the specificity of compound **11** to illuminate mitochondria in cancer cells over non-cancerous cells by confocal microscopy. Non-cancerous fibroblast L929 cells were treated with compound **11** at 20 µM concentration followed by staining nuclei and mitochondria by DAPI (blue) and MitoTracker Red (red). The confocal microscopy images (Figure 39b) barely showed any green or yellow fluorescence signal inside the cells or in mitochondria respectively. This microscopy experiment established that compound **11** is highly specific for mitochondria in HeLa cancer cells compared to non-cancerous L929 cells at much lower concentration compared to Rhodamine 123.[46]

In conclusion, we have synthesized hydrazide-hydrazone based small molecules in concise and easy steps in high yield, which demonstrated for the first time remarkable aggregation-induced emission (AIE) property in water as well as in solid state. Theoretical calculation, crystal structure, proton-NMR spectroscopy along with reversible temperature and pH dependent studies confirmed that dual intra-molecular H-bonding was responsible for restricting the intra-molecular motion to show this hitherto unobserved AIE property. A triphenylphosphonium labeled hydrazide-hydrazone AIEgen was synthesized to illuminate mitochondria in HeLa cells selectively. These novel biocompatible hydrazide-hydrazone small molecules can be used as platform to develop innovative AIEgens to image different sub-cellular organelles and targets in cancer cells as future theranostic strategies by incorporating photothermal and photo-dynamic probes.

Acknowledgements

S.B. thanks Department of Biotechnology for Ramalingaswami Fellowship (BT/RLF/Re-entry/13/2011) and other financial supports (BT/PR9918/NNT/28/692/2013, and BT/PR14724/NNT/28/831/2015). S. Patil and S. Pandey acknowledge CSIR-UGC and IISER-Pune for doctoral fellowship respectively. We sincerely thank Mr. Ravindra Raut of IISER-Pune for helping in X-ray crystallography analysis. A.S and M.R thank the High Performance Computing facility at IIT Gandhinagar for computational resources.

Keywords: Hydrazide-hydrazone • aggregation-induced emission • H-bonding • mitochondria • cancer

[1] J. Mei, N. L. C. Leung, R. T. K. Kwok, J. W. Y. Lam, B. Z. Tang! *Chem. Rev.* **2015**, *115*, 11718-11940.
[2] B. Liu, R. Zhang, *Faraday Discussion* **2017**, *196*, 461-472.
[3] X. Jiang, H. Gao, X. Zhang, J. Pang, Y. Li, K. Li, Y. Wu, S. Li, J. Zhu, Y. Wei, L. Jiang, *Nat. Commun*. **2018**, *9*, 3799.
[4] Y. Chen, X. Min, X, Zhang, F. Zhang, S. Lu. L. Xu, X. Lou, F. Xia, X. Zhang, S. Wang, *Biosens. Bioelectron*. **2018**, *111*, 124-130.
[5] J. Qi, C. Chen, D. Ding, B. Z. Tang, *Adv. Healthc. Mater.* **2018**, *7*, e1800477.
[6] C. Zhu, R. T. K. Kwok, J. W. Y. Lam, B. Z. Tang, *ACS Appl. Bio. Mater.* **2018**, *1*, 1768-1786.
[7] Y. Hong, J. W. Y. Lam, B. Z. Tang, *Chem. Commun*. **2009**, *0*, 4332-4353.
[8] Y. Hong, J. W. Y. Lam, B. Z. Tang, *Chem. Soc. Rev*. **2011**, *40*, 5361-5388.
[9] D. Ding, K. Li, B. Liu, B. Z. Tang, *Acc. Chem. Res*. **2013**, *46*, 2441-2453.
[10] J. Mei, Y. Hong, J. W. Y. Lam, A. Qin, Y. Tang, B. Z. Tang, *Adv. Mater.* **2014**, *26*, 5429-5479.
[11] Y. Chen, W. Zhang, Z. Zhao, Y. Cai, J. Gong, R. T. K. Kwok, J. W. Y. Lam, H. H. Y. Sung, I. D. Williams, B. Z. Tang, *Angew Chem. Int. Ed.* **2018**, *57*, 5011-5015.
[12] Y. Hong, S. Chen, C. Wai, T. Leung, J. Wing, Y. Lam, B. Z. Tang, *Chem. Asian J.* **2013**, *8*, 1806-1812.
[13] H. Shi, R. T. K. Kwok, J. Liu, B. Xing, B. Z. Tang, B. Liu, *J. Am. Chem. Soc.* **2012**, *134*, 17972-17981.
[14] G. Jiang, G. Zeng, W. Zhu, Y. Li, X. Dong, G. Zhang, X. Fan, J. Wang, Y. Wu, B. Z. Tang, *Chem. Commun.* **2017**, *53*, 4505-4508.
[15] F. Hu, D. Mao, Kenry, X. Cai, W. Wu, D. Kong, B. Liu, *Angew Chem. Int. Ed.* **2018**, *57*, 10182-10186.
[16] F. Hu, B. Liu, *Org. Biomol. Chem*. **2016**, *14*, 9931-9944.
[17] J. Qian, B. Z. Tang, *Chem* **2017**, *3*, 56-91.
[18] G. Niu, R. Zhang, J. P. C. Kwong, J. W. Y. Lam, C. Chen, J. Wang, Y. Chen, X. Feng, R. T. K. Kwok, H. H.-Y. Sung, I. D. Williams, M. R. J. Elsegood, J. Qu, C. Ma, K. S. Wong, X. Yu, B. Z. Tang, *Chem. Mater*. **2018**, *30*, 4778–4787.
[19] Y. Cai, C. Gui, K. Samedov, H. Su, X. Gu, S. Li, W. Luo, H. H. Y. Sung, J. W. Y. Lam, R. T. K. Kwok, I. D. Williams, A. Qin, B. Z. Tang, *Chem. Sci.* **2017**, *8*, 7593-7603.

[20] Y. Li, Y. Wu, J. Chang, M. Chen, R. Liu, F. Li, *Chem. Commun*. **2013**, *49*, 11335-11337.
[21] C. Y. Y. Yu, W. Zhang, R. T. K. Kwok, C. W. T. Leung, J. W. Y. Lam, B. Z. Tang, *J. Mater. Chem. B* **2016**, *4*, 2614-2619.
[22] D. C. Wallace, *Nat. Rev. Cancer* **2012**, *12*, 685-698.
[23] S. Fulda, L. Galluzzi, G. Kroemer, *Nat. Rev. Drug Discovery* **2010**, *9*, 447-464.
[24] J. Nunnari, A. Suomalainen, *Cell* **2012**, *148*, 1145-1159.
[25] N. Zhao, M. Li, Y. Yan, J. W. Y. Lam, Y. L. Zhang, Y. S. Zhao, K. S. Wong, B. Z. Tang, *J. Mater. Chem. C* **2013**, *1*, 4640-4646.
[26] C. W. T. Leung, Y. Hong, S. Chen, E. Zhao, J. W. Y. Lam, B. Z. Tang, *J. Am. Chem. Soc.* **2013**, *135*, 62-65.
[27] M. Gao, C. K. Sim, C. W. T. Leung, Q. Hu, G. Feng, F. Xu, B. Z. Tang, B. Liu, *Chem. Commun.* **2014**, *50*, 8312-8315.
[28] W. Zhang, R. T. K. Kwok, Y. Chen, S. Chen, E. Zhao, C. Y. Y. Yu, J. W. Y. Lam, Q. Zheng, B. Z. Tang, *Chem. Commun.* **2015**, *51*, 9022-9025.
[29] Q. Hu, M. Gao, G. Feng, B. Liu, *Angew. Chem. Int. Ed.* **2014**, *53*, 14225-14229.
[30] G. Yu, D. Wu, Y. Li, Z. Zhang, L. Shao, J. Zhou, Q. Hu, G. Tang, F. Huang, *Chem. Sci.* **2016**, *7*, 3017-3024.
[31] O. G. Tsay, S. T. Manjare, H. Kim, K. M. Lee, Y. S. Lee, D. G. Churchill, *Inorg. Chem.* **2013**, *52*, 10052−10061
[32] M. Savarese, A. Aliberti, I. D. Santo, E, Battista, F, Causa, P, A. Netti, N. Rega, *J. Phys. Chem. A.* **2012**, *116*, 7491-7497.
[33] Q. Feng, Y. Li, L. Wang, C. Li, J. Wang, Y. Liu, K. Li, H, Hou, *Chem. Commun*. **2016**, *52*, 3123-3126.
[34] M. J. Frisch, G. W. Trucks, H. B. Schlegel, G. E. Scuseria, M. A. Robb, J. R. Cheeseman, G. Scalmani, V. Barone, B. Mennucci, G. A. Petersson, Gaussain 09, Revision D. 01; Gaussian. *Inc.: Wallingford, CT, USA*, **2013**.
[35] P. J. Stephens, F. J. Devlin, C. F. N. Chabalowski, M. J. Frisch, *J. Phys. Chem.* **1994**, *98*, 11623-11627.
[36] S. Miertuš, E. Scrocco, J. Tomasi, *Chem. Phys.* **1981**, *55*, 117-129.
[37] Q. Yuan, T. Zhou, L. Li, J. Zhang, X. Liu, X. Ke, A. Zhang, *RSC Adv.* **2015**, *5*, 31153-31165.
[38] N. Avakyan, A. A. Greschner, F. Aldaye, C. J. Serpell, V. Toader, A. Petitjean, H. F. Sleiman, *Nat. Chem.* **2016**, *8*, 368-376
[39] C. Ghosh, A. Nandi, S, Basu, *Nanoscale* **2019**, *11*, 3326-3335
[40] M. S. Mathew, K. Sreenivasan, K. Joseph, *RSC Adv.* **2015**, *5*, 100176.
[41] J. Zhao, S. Ji, Y.Chen, H. Guo P.Yang, *Phys. Chem. Chem. Phys*. **2012**, *14*, 8803-8817.
[42] A. C. Sedgwick, L. Wu, H-H. Han, S. D. Bull, X-P. He, T. D. James, J. L. Sessler, B. Z. Tang, H. Tian, J. Yoon, *Chem. Soc. Rev.* **2018**, *47*, 8842- 8880
[43] S. Patil, M. M. Kuman, S. Palvai, P. Sengupta, S. Basu, *ACS Omega*, **2018**, *3*, 1470-1481.
[44] J. S. Modica-Napolitano, J. R. Aprille, *Cancer Res*. **1987**, *47*, 4361-4365.
[45] W. H. Goffney, J. H. Wong, D. H. Kern, D. Chase, D. N. Krag, F. K. Storm, *Cancer Res.* **1990**, 50, 459-463.
[46] L. V. Johnson, M. L. Walsh, and L. B. Chen, *Proc. Natl. Acad. Sci. USA*, **1980**, *77*, 990-994.

10.1002/chem.201901074

WILEY-VCH

Entry for the Table of Contents (Please choose one layout)

COMMUNICATION

Light up the powerhouse: Biocompatible hydrazide-hydrazones showed remarkable aggregation-induced emission (AIE) through dual intra-molecular H-bonding to illuminate the powerhouse (mitochondrion) in cancer cells.

Sohan Patil,[a] Shalini Pandey,[a] Amit Singh,[b] Mithun Radhakrishna,[c] and Sudipta Basu[b]*

Page No. – Page No.

Hydrazide-hydrazone Small Molecules as AIEgens: Illuminating Mitochondria in Cancer Cells